

**DEVELOPMENT OF RARE-EARTH FREE PERMANENT
MAGNETS WITH IMPROVED MAGNETIC PROPERTIES**



**Thesis submitted in partial fulfillment
for the Award of Degree**

DOCTOR OF PHILOSOPHY

By

AKANKSHA GUPTA

DEPARTMENT OF CERAMIC ENGINEERING

**INDIAN INSTITUTE OF TECHNOLOGY
(BANARAS HINDU UNIVERSITY)
VARANASI – 221005**

INDIA

18031007

2022



भारतीय
प्रौद्योगिकी
संस्थान
काशी हिन्दू विश्वविद्यालय




INDIAN
INSTITUTE OF
TECHNOLOGY
BANARAS HINDU UNIVERSITY

CERTIFICATE

It is certified that the work contained in the thesis titled "**Development of Rare-Earth Free Permanent Magnets with Improved Magnetic Properties**" by "**AKANKSHA GUPTA**" has been carried out under my supervision and that this work has not been submitted elsewhere for a degree.

It is further certified that the student has fulfilled all the requirements of Comprehensive Examination, Candidacy and SOTA for the award of Ph.D. Degree.


Dr. Pradip Kumar Roy
(Supervisor)

Dr. Pradip Kumar Roy
Associate Professor
Department of Ceramic Engineering,
Indian Institute of Technology (I.I.T) (BHU),
Banaras Hindu University, Varanasi-221005
Uttar Pradesh (U.P.), INDIA



भारतीय
प्रौद्योगिकी
संस्थान
काशी हिन्दू विश्वविद्यालय



INDIAN
INSTITUTE OF
TECHNOLOGY
BANARAS HINDU UNIVERSITY

DECLARATION BY THE CANDIDATE

I, **AKANKSHA GUPTA**, certify that the work embodied in this thesis is my own bona fide work and carried out by me under the supervision of **DR. PRADIP KUMAR ROY** from July, 2018 to November, 2022 at the Department of Ceramic Engineering, Indian Institute of Technology (BHU), Varanasi. The matter embodied in this thesis has not been submitted for the award of any other degree/diploma. I declare that I have faithfully acknowledged and given credits to the research workers wherever their works have been cited in my work in this thesis. I further declare that I have not willfully copied any other's work, paragraphs, text, data, results, etc., reported in journals, books, magazines, reports dissertations, theses, etc., or available at websites and have not included them in this thesis and have not cited as my own work.

Date : November 10, 2022

Place: IIT (BHU), Varanasi

Akanksha Gupta

AKANKSHA GUPTA

CERTIFICATE BY THE SUPERVISOR

It is certified that the above statement made by the student is correct to the best of my knowledge.

Pradip Kumar Roy

Dr. Pradip Kumar Roy
(Supervisor)

Dr. Pradip Kumar Roy
Associate Professor
Department of Ceramic Engineering,
Indian Institute of Technology (I.I.T) (BHU),
Banaras Hindu University, Varanasi-221005
Uttar Pradesh (U.P.), INDIA

Vinay Kumar Singh

Prof. Vinay Kumar Singh
(Head of Department)

HEAD/ विभागाध्यक्ष
Department of Ceramic Engineering
सिरामिक अभियान्त्रिकी विभाग
Indian Institute of Technology (B.H.U.)
भारतीय प्रौद्योगिकी संस्थान (का.हि.वि.वाराणसी)
Varanasi-221005/ वाराणसी-221005



COPYRIGHT TRANSFER CERTIFICATE

Title of the Thesis : Development of Rare-Earth Free Permanent Magnets with Improved Magnetic Properties

Name of the Student : Akanksha Gupta

Copyright Transfer

The undersigned hereby assigns to the Indian Institute of Technology (Banaras Hindu University), Varanasi all rights under copyright that may exist in and for the above thesis submitted for the award of the Doctor of Philosophy.

Date : November 10, 2022

Place: IIT (BHU), Varanasi



AKANKSHA GUPTA

Note: However, the author may reproduce or authorize others to reproduce material extracted verbatim from the thesis or derivative of the thesis for author's personal use provided that the source and the Institute's copyright notice are indicated

Dedicated to My Grandfather
Late Mr. Moti Narayan

&
My Beloved Family

ACKNOWLEDGEMENTS

"We should not give up and we should not allow the problem to defeat us"- Dr. A.P.J. Abdul Kalam. This line expresses the journey of doctoral life, which is full of challenges and difficulties. Life is nothing without experience, and I am fortunate to possess a wonderful journey at IIT (BHU). I get the direct and indirect support of many people around me to accomplish this journey successfully. It is my immense pleasure to get the mammoth opportunity to thank those people to whom I will be grateful forever.

At the very beginning, I would like to express my thankfulness to Mahamana Pandit Madan Mohan Malviya, founder of BHU, for his contribution to the education and IIT (BHU), Varanasi, where I have spent a precious time of my life. This place provided me with many learnings of life and its beautiful campus gave me a delightful environment to positively carry out my research work.

I wish to express my sincere gratitude and respect to my research supervisor Dr. Pradip Kumar Roy, Department of Ceramic Engineering, IIT (BHU), for giving me the opportunity to work under his esteemed guidance. I must appreciate him for providing me the prospects to think, work, and express my research work by keeping faith in my capabilities. Moreover, his valuable insights on various technical ideas and his colossal experience in the magnetic material field helped me to sort out research problems that arose in the experimentations.

I am highly grateful to my doctoral committee members, Dr. Mohammad Imteyaz Ahmad and Dr. Shravan Kumar Mishra, for their valuable suggestions and feedback to improve my research work from various perspectives. I express my sincere gratitude to the present Head of Department (HoD), Ceramic Engineering, Prof. Vinay Kumar Singh and former HoDs, Prof. Devendra Kumar, Prof. Ram Pyare, for providing me with various departmental facilities. I am also thankful to all the faculty members and other staff members of the Department of Ceramic Engineering as well.

I wish to convey a special thanks to the Incharge (Prof. Rajiv Prakash) and all the technical staff of Central Instrument Facility (CIF), IIT (BHU) for availing me of various instrumental facilities. I am very much thankful to Dr. Manoranjan Kar, IIT Patna, for his help in magnetic measurements of Cr-Zn and Ni-Al substituted SrM samples.

I would like to extend my sincere gratitude to the Department of Science and Technology (DST), New Delhi (Ref No: IMP/2019/000165) and IIT (BHU) for providing me with financial support for this thesis.

I am fortunate to have labmates Dr. Deepshikha Shekhawat, Dr. Priyanka Verma, Dr. SK Saddam Hossain, Mr. Satyendra Kumar Singh, Mr. Soham Mukherjee, Mr. Sandip Kumar Patel, Mr. Sumit Kumar Singh, and Mr. Akash Sahu who will always be remembered for the wonderful time we shared together. "Life without Friends is like sweet without sugar." I am very grateful to have many of them. I am greatly thankful to my friends, Dr. Mukesh Suthar, Dr. Debarati Pal, Dr. Shanu Mishra, Mrs. Priya Singh, Mr. Pawan Kumar, Mrs. Jyoti Sharma, Mr. Pratyush Shukla, Mrs. Anviti Pandey, Dr. Manisha Singla, Mrs. Mahima Singh, Mrs. Arpita Gupta, and others for adding sparkles in my life.

Family is the biggest blessing that builds the individual's personality and helps one to become strong and vibrant. I would like to express my special gratitude to the greatest strength of my life, my parents (Mr. Vinay Narayan and Ms. Sunita Gupta) and my siblings (Dr. Saksham Gupta and Ms. Samridhi Gupta) for being the backbone of my journey. I am very much grateful to Mr. Atharva, my Dadi (Late Mrs. Chandramukhi Devi), my family members, my Nani, and relatives for their love, care, blessings, and constant support throughout my life.

At last, my heartiest gratitude to the almighty God for giving me all the strength and courage to face all the difficulties and giving me the opportunity to enjoy this beautiful journey of life with zeal and zest.

Date : November 10, 2022

Place: IIT (BHU), Varanasi

*Akanksha
Gupta*

AKANKSHA GUPTA

Table of Contents

Certificate	iii
Declaration by the Candidate	v
Copyright Transfer Certificate	vii
Acknowledgements	xi
Table of Contents	xiii
List of Figures	xvii
List of Tables	xxi
List of Abbreviations and Symbols	xxiii
Preface	xxv
Chapter 1: Introduction and Literature Survey	1-30
1.1 Introduction	1
1.2 Overview of Magnetic Parameters	3
1.3 Strontium Hexaferrite Magnet	8
1.4 Criteria for Development of Permanent Magnet	10
1.5 Literature Survey on Synthesis Techniques for SrM	11
1.5.1 Solid-state Reaction Process	12
1.5.2 Hydrothermal Process	13
1.5.3 Co-precipitation Process	14
1.5.4 Sol-gel Process	15
1.5.5 Sol-gel Auto-combustion method	16
1.6 Literature Survey on Substitutional Efficacy of Non-REEs in SrM	17
1.7 Scope and Objective of the Present Work	29
Chapter 2: Experimental Techniques	31-47
2.1 Sample Preparation	31
2.1.1 Solid-state Reaction Route (Traditional Ceramic Method)	31
2.1.2 Sol-gel Auto-combustion Process	33
2.1.3 Heat Treatment Process	35
2.2 Characterization Techniques	36
2.2.1 Differential Thermal Analyzer & Thermo-gravimetric (DTA-TG)	36
2.2.2 X-ray Diffraction (XRD)	37
2.2.3 Fourier Transform Infrared Spectroscopy (FTIR)	39
2.2.4 Scanning Electron Microscopy (SEM)	41
2.2.5 Bulk Density and Porosity	43
2.2.6 Superconducting Quantum Interference Device Magnetometer	43
2.2.7 Impedance Analyzer	46
Chapter 3: Co-Cr Substituted SrFe_{12-x-y}Co_xCr_yO₁₉ Series	49-63
3.1 Introduction	49
3.2 Results and Discussion	49
3.2.1 TG/DTA Analysis	49
3.2.2 Structural Properties	50
3.2.3 Spectroscopic Properties	52

3.2.4	Densification and Microstructural Properties	54
3.2.5	Magnetic Properties	55
3.2.6	Dielectric Properties	59
3.2.7	Electrical Properties	62
3.3	Conclusions	63
Chapter 4: Cr-Zn Substituted Sr_{1-x}Cr_xFe_{12-x}Zn_xO₁₉ Series		65-79
4.1	Introduction	65
4.2	Results and Discussion	65
4.2.1	Structural Properties	65
4.2.2	Spectroscopic Properties	67
4.2.3	Densification and Microstructural Properties	69
4.2.4	Magnetic Properties	71
4.2.5	Dielectric Properties	75
4.2.6	Electrical Properties	77
4.3	Conclusions	78
Chapter 5: Ni-Al Substituted SrFe_{12-x-y}Ni_xAl_yO₁₉ Series		81-97
5.1	Introduction	81
5.2	Results and Discussion	82
5.2.1	Structural Properties	82
5.2.2	Spectroscopic Properties	84
5.2.3	Densification and Microstructural Properties	86
5.2.4	Magnetic Properties	88
5.2.5	Dielectric Properties	91
5.2.6	Electrical Properties	95
5.3	Conclusions	96
Chapter 6: Bi₂O₃ Doped SrFe₈Al₄O₁₉ Series		99-116
6.1	Introduction	99
6.2	Results and Discussion	100
6.2.1	Analysis of SrFe ₈ Al ₄ O ₁₉ Raw Powder	100
6.2.2	Analysis of SrFe ₈ Al ₄ O ₁₉ Calcined Powder	101
6.2.3	Analysis of SrFe ₈ Al ₄ O _{19-x} Bi ₂ O ₃ (0 ≤ x ≤ 5 wt%) Sintered Pellets	102
6.2.3.1	Structural Properties	102
6.2.3.2	Densification and Microstructural Properties	103
6.2.3.3	Magnetic Properties	106
6.2.3.4	Dielectric Properties	110
6.2.3.5	Electrical Properties	113
6.3	Conclusions	116
Chapter 7: Al-Zn Substituted SrFe_{8-x}Al₄Zn_xO₁₉ Series		117-132
7.1	Introduction	117
7.2	Results and Discussion	118

7.2.1 Structural Properties	118
7.2.2 Spectroscopic Properties	119
7.2.3 Densification and Microstructural Properties	121
7.2.4 Magnetic Properties	123
7.2.5 Dielectric Properties	127
7.2.6 Electrical Properties	131
7.3 Conclusions	132
Chapter 8: Progress in Energy Density	133-140
8.1 Introduction	133
8.2 Calculation of Energy Density	133
8.3 Energy density and Curie Temperature	134
8.3.1 A Composition of SrFe ₈ Al ₄ O ₁₉ _3 wt% Bi ₂ O ₃ , (1050°C)	134
8.3.2 A Composition of SrFe _{8.985} Ni _{0.015} Al ₃ O ₁₉	136
8.3.3 A Composition of SrFe _{7.8} Al ₄ Zn _{0.2} O ₁₉	138
8.4 Conclusions	139
Chapter 9: Summary and Future Scope	141-145
9.1 Summary	141
9.2 Future Scope	144
References	147-161
List of Publications and Patents	163
Attended International Conferences	165

List of Figures

Figure 1.1 Applications of PMs by market share, market dominancy and production of different PMs in 2019.	2
Figure 1.2 Dependency of coercivity on grain size D ; D_{spm} is the critical grain size that results in superparamagnetism, and D_s is the critical grain size for the single domain.	6
Figure 1.3 M-type hexagonal structure of strontium hexaferrite.	9
Figure 1.4 Structure of S (spinel layer of $Fe_6O_8^{2+}$) & R (hexagonal layer of $SrFe_6O_{11}^{2-}$) blocks.	9
Figure 1.5 Variation in H_c parameter with Al-substitution in $SrFe_{12-x}Al_xO_{19}$.	22
Figure 1.6 Variation pattern of H_c with Al substitution and annealing temperature (T_{ann}) in SrM.	22
Figure 2.1 Schematic diagram of traditional solid-state reaction route.	32
Figure 2.2 Schematic diagram of a sol-gel auto-combustion process.	34
Figure 2.3 Schematic representation of controlled muffle furnace.	36
Figure 2.4 Schematic representation of DTA and TGA.	37
Figure 2.5 Schematic representation of Bragg-Brentano geometry (Ray diagram of XRD) and Bragg's law.	39
Figure 2.6 Schematic representation of Fourier transform infrared spectroscopy.	40
Figure 2.7 Schematic representation of scanning electron microscope.	42
Figure 2.8 Schematic representation of electron interaction with sample along with different generated signals.	42
Figure 2.9 A simplified representation of the SQUID magnetometer.	45
Figure 2.10 Schematic representation of working principle of SQUID.	45
Figure 2.11 Schematic representation of room-temperature impedance analyzer.	47
Figure 3.1 TG/DTA curve of $SrFe_{12}O_{19}$ dried sol-gel.	50
Figure 3.2 XRD patterns of calcined $SrFe_{12-x-y}Co_xCr_yO_{19}$ ($0 \leq x, y \leq 1$) hexaferrites.	51
Figure 3.3 FT-IR spectra of calcined $SrFe_{12-x-y}Co_xCr_yO_{19}$ ($0 \leq x, y \leq 1$) hexaferrites.	53
Figure 3.4 SEM micrographs of a) $SrFe_{12}O_{19}$, b) $SrFe_{11}CrO_{19}$, c) $SrFe_{11}Co_{0.25}Cr_{0.75}O_{19}$, d) $SrFe_{11}Co_{0.5}Cr_{0.5}O_{19}$, e) $SrFe_{11}Co_{0.75}Cr_{0.25}O_{19}$, and f) $SrFe_{11}CoO_{19}$ hexaferrites.	55

Figure 3.5 *M-H hysteresis curve of $SrFe_{12-x-y}Co_xCr_yO_{19}$ ($0 \leq x, y \leq 1$) hexaferrites.* 56

Figure 3.6. *M vs. $1/H^2$ plot with $S-W$ linear fitting for $SrFe_{12-x-y}Co_xCr_yO_{19}$ ($0 \leq x, y \leq 1$) hexaferrites.* 58

Figure 3.7 *Dielectric constant (ϵ) of $SrFe_{12-x-y}Co_xCr_yO_{19}$ ($0 \leq x, y \leq 1$) hexaferrites with respect to frequency at room-temperature.* 60

Figure 3.8 *Dielectric loss ($\tan\delta$) of $SrFe_{12-x-y}Co_xCr_yO_{19}$ ($0 \leq x, y \leq 1$) hexaferrites with respect to frequency at room-temperature.* 61

Figure 3.9 *Ac-resistivity (ρ) of $SrFe_{12-x-y}Co_xCr_yO_{19}$ ($0 \leq x, y \leq 1$) hexaferrites with respect to frequency.* 62

Figure 4.1 *XRD patterns of $Sr_{1-x}Cr_xFe_{12-y}Zn_yO_{19}$ ($0 \leq x \leq 0.8; 0 \leq y \leq 1$) hexaferrites.* 66

Figure 4.2 *FT-IR spectra of calcined $Sr_{1-x}Cr_xFe_{12-y}Zn_yO_{19}$ ($0 \leq x \leq 0.8; 0 \leq y \leq 1$) hexaferrites.* 68

Figure 4.3 *SEM micrographs of a) $SrCr_{0.2}Fe_{12}O_{19}$, b) $SrCr_{0.2}Fe_{11.8}Zn_{0.2}O_{19}$, c) $SrCr_{0.4}Fe_{11.6}Zn_{0.4}O_{19}$, d) $SrCr_{0.6}Fe_{11.4}Zn_{0.6}O_{19}$, e) $SrCr_{0.8}Fe_{11.2}Zn_{0.8}O_{19}$, and f) $SrFe_{11}ZnO_{19}$ hexaferrites.* 70

Figure 4.4 *$M-H$ hysteresis curve of $Sr_{1-x}Cr_xFe_{12-y}Zn_yO_{19}$ ($0 \leq x \leq 0.8; 0 \leq y \leq 1$) hexaferrites.* 72

Figure 4.5 *M vs. $1/H^2$ plot with $S-W$ linear fitting for $Sr_{1-x}Cr_xFe_{12-y}Zn_yO_{19}$ ($0 \leq x \leq 0.8; 0 \leq y \leq 1$) hexaferrites.* 74

Figure 4.6 *Dielectric constant (ϵ) of $Sr_{1-x}Cr_xFe_{12-y}Zn_yO_{19}$ ($0 \leq x \leq 0.8; 0 \leq y \leq 1$) hexaferrites with respect to frequency at room-temperature.* 76

Figure 4.7 *Dielectric loss ($\tan\delta$) of $Sr_{1-x}Cr_xFe_{12-y}Zn_yO_{19}$ ($0 \leq x \leq 0.8; 0 \leq y \leq 1$) hexaferrites with respect to frequency at room-temperature.* 76

Figure 4.8 *Frequency-dependent resistivity variation in $Sr_{1-x}Cr_xFe_{12-y}Zn_yO_{19}$ ($0 \leq x \leq 0.8; 0 \leq y \leq 1$) hexaferrites.* 78

Figure 5.1 *Progress in coercivity (H_c , kOe) & saturation magnetization (M_s , emu/g) of $SrFe_8Al_4O_{19}$ hexaferrite with different synthesis processes, T_{ann} , T_{cal} , and T_{sin} .* 82

Figure 5.2 *XRD patterns of $SrFe_{12-x-y}Ni_xAl_yO_{19}$ ($0.005 \leq x \leq 0.02; 1 \leq y \leq 4$) hexaferrite.* 83

Figure 5.3 *FT-IR spectra of calcined $SrFe_{12-x-y}Ni_xAl_yO_{19}$ ($0.005 \leq x \leq 0.02; 1 \leq y \leq 4$) hexaferrites.* 85

Figure 5.4 *SEM micrographs of a) $SrFe_{11.99}Ni_{0.01}O_{19}$, b) $SrFe_{11}AlO_{19}$, c) $SrFe_{10.995}Ni_{0.005}AlO_{19}$, d) $SrFe_{9.99}Ni_{0.01}Al_2O_{19}$, e) $SrFe_{8.985}Ni_{0.015}Al_3O_{19}$, and f) $SrFe_{7.98}Ni_{0.02}Al_4O_{19}$ hexaferrites.* 87

Figure 5.5 <i>M-H hysteresis curve of $SrFe_{12-x-y}Ni_xAl_yO_{19}$ ($0.005 \leq x \leq 0.02$; $1 \leq y \leq 4$) hexaferrites.</i>	88
Figure 5.6. <i>M vs $1/H^2$ plot with linear fit for $SrFe_{12-x-y}Ni_xAl_yO_{19}$ ($0.005 \leq x \leq 0.02$; $1 \leq y \leq 4$) hexaferrites.</i>	91
Figure 5.7 <i>Dielectric constant (ϵ) of $SrFe_{12-x-y}Ni_xAl_yO_{19}$ ($0.005 \leq x \leq 0.02$; $1 \leq y \leq 4$) hexaferrites with respect to frequency at room-temperature.</i>	92
Figure 5.8 <i>Schematic of polarization occurrence due to distorted oxygen octahedron.</i>	92
Figure 5.9 <i>Dielectric loss ($\tan\delta$) of $SrFe_{12-x-y}Ni_xAl_yO_{19}$ ($0.005 \leq x \leq 0.02$; $1 \leq y \leq 4$) hexaferrites with respect to frequency at room-temperature.</i>	94
Figure 5.10 <i>Frequency-dependent resistivity variation in $SrFe_{12-x-y}Ni_xAl_yO_{19}$ ($0.005 \leq x \leq 0.02$; $1 \leq y \leq 4$) hexaferrites.</i>	96
Figure 6.1 <i>TG/DTA curve of $SrFe_8Al_4O_{19}$ raw powder.</i>	101
Figure 6.2 <i>(a) FT-IR spectra and (b) XRD pattern of $SrFe_8Al_4O_{19}$ calcined powder.</i>	101
Figure 6.3 <i>XRD pattern of $SrFe_8Al_4O_{19-x}Bi_2O_3$ ($0 \leq x \leq 5$ wt%) hexaferrites sintered at $1050^\circ C$ temperature.</i>	103
Figure 6.4 <i>SEM images of $SrFe_8Al_4O_{19-x}Bi_2O_3$ ($x = 3$ wt%) hexaferrite sintered at $850^\circ C$ to $1150^\circ C$.</i>	104
Figure 6.5 <i>SEM images of $SrFe_8Al_4O_{19-x}Bi_2O_3$ ($0 \leq x \leq 5$ wt%) hexaferrite sintered at $1050^\circ C$.</i>	104
Figure 6.6 <i>Hysteresis curve of $SrFe_8Al_4O_{19-x}Bi_2O_3$ ($0 \leq x \leq 5$ wt%) hexaferrites sintered at $850^\circ C$-$1150^\circ C$ sintering temperature.</i>	108
Figure 6.7 <i>Variation in M_s and H_c of $SrFe_8Al_4O_{19-x}Bi_2O_3$ ($0 \leq x \leq 5$ wt%) hexaferrites with different Bi_2O_3 content and sintering temperatures.</i>	108
Figure 6.8 <i>Frequency-dependent dielectric constant behavior of $SrFe_8Al_4O_{19-x}Bi_2O_3$ ($0 \leq x \leq 5$ wt%) hexaferrites with different Bi_2O_3 content and at different sintering temperatures.</i>	110
Figure 6.9 <i>Frequency-dependent dielectric loss ($\tan\delta$) of $SrFe_8Al_4O_{19-x}Bi_2O_3$ ($0 \leq x \leq 5$ wt%) hexaferrites with different Bi_2O_3 content and at different sintering temperatures.</i>	112
Figure 6.10 <i>Frequency-dependent ac resistivity of $SrFe_8Al_4O_{19-x}Bi_2O_3$ ($0 \leq x \leq 5$ wt%) hexaferrites with different Bi_2O_3 content and at different sintering temperatures.</i>	114
Figure 7.1 <i>XRD patterns of $SrFe_{8-x}Al_4Zn_xO_{19}$ ($0 \leq x \leq 1$) hexaferrites.</i>	118

- Figure 7.2** FT-IR spectra of calcined $\text{SrFe}_{8-x}\text{Al}_4\text{Zn}_x\text{O}_{19}$ ($0 \leq x \leq 1$) hexaferrites. 120
- Figure 7.3** SEM micrographs of a) $\text{SrFe}_8\text{Al}_4\text{O}_{19}$, b) $\text{SrFe}_{7.8}\text{Al}_4\text{Zn}_{0.2}\text{O}_{19}$, c) $\text{SrFe}_{7.6}\text{Al}_4\text{Zn}_{0.4}\text{O}_{19}$, d) $\text{SrFe}_{7.4}\text{Al}_4\text{Zn}_{0.6}\text{O}_{19}$, e) $\text{SrFe}_{7.2}\text{Al}_4\text{Zn}_{0.8}\text{O}_{19}$, and f) $\text{SrFe}_7\text{Al}_4\text{ZnO}_{19}$ hexaferrites. 122
- Figure 7.4** M-H hysteresis curve of $\text{SrFe}_{8-x}\text{Al}_4\text{Zn}_x\text{O}_{19}$ ($0 \leq x \leq 1$) hexaferrites. 123
- Figure 7.5** M vs $1/H^2$ plot with linear fit for $\text{SrFe}_{8-x}\text{Al}_4\text{Zn}_x\text{O}_{19}$ ($0 \leq x \leq 1$) hexaferrite. 126
- Figure 7.6** Dielectric constant (ϵ) of $\text{SrFe}_{8-x}\text{Al}_4\text{Zn}_x\text{O}_{19}$ ($0 \leq x \leq 1$) hexaferrites with respect to frequency at room-temperature. 128
- Figure 7.7** Dielectric loss ($\tan\delta$) of $\text{SrFe}_{8-x}\text{Al}_4\text{Zn}_x\text{O}_{19}$ ($0 \leq x \leq 1$) hexaferrite with respect to frequency at room-temperature. 128
- Figure 7.8** Frequency-dependent resistivity variation in $\text{SrFe}_{8-x}\text{Al}_4\text{Zn}_x\text{O}_{19}$ ($0 \leq x \leq 1$) hexaferrites. 131
- Figure 8.1** Energy density $(BH)_{\max}$ of $\text{SrFe}_8\text{Al}_4\text{O}_{19-x}\text{Bi}_2\text{O}_3$ ($x = 3$ wt%) hexaferrite sintered at 1050°C , estimated from demagnetization curve, where iH_c is intrinsic coercivity & bH_c is magnetic induction coercivity. 135
- Figure 8.2** M-T curve of $\text{SrFe}_8\text{Al}_4\text{O}_{19-x}\text{Bi}_2\text{O}_3$ ($x = 3$ wt%) hexaferrite sintered at 1050°C . 135
- Figure 8.3** Energy density $(BH)_{\max}$ of $\text{SrFe}_{8.985}\text{Ni}_{0.015}\text{Al}_3\text{O}_{19}$ hexaferrite, estimated from demagnetization curve, where iH_c is intrinsic coercivity & bH_c is magnetic induction coercivity. 136
- Figure 8.4** M-T curve of $\text{SrFe}_{8.985}\text{Ni}_{0.015}\text{Al}_3\text{O}_{19}$ hexaferrite magnet. 137
- Figure 8.5** Energy density $(BH)_{\max}$ of $\text{SrFe}_{7.8}\text{Al}_4\text{Zn}_{0.2}\text{O}_{19}$ hexaferrite, estimated from demagnetization curve, where iH_c is intrinsic coercivity & bH_c is magnetic induction coercivity. 139
- Figure 8.6** M-T curve of $\text{SrFe}_{7.8}\text{Al}_4\text{Zn}_{0.2}\text{O}_{19}$ hexaferrite magnet. 139

List of Tables

Table 1.1 Comparison of magnetic properties and price of different commercial permanent magnets.	3
Table 1.2 Different lattice sites for Fe ion distribution in M-type hexaferrite.	10
Table 1.3 Comparison of various synthesis routes of SrM magnet with magnetic properties.	17
Table 1.4 Compiled substitutional effect of various non-rare-earth elements in magnetic properties of SrM with M_s and H_c values.	27
Table 3.1 Structural parameters of $SrFe_{12-x-y}Co_xCr_yO_{19}$ ($0 \leq x, y \leq 1$) hexaferrites.	52
Table 3.2 Characteristic absorption peaks [ν_1 , ν_2 (tetrahedral) & ν_3 (octahedral)] and bond length (r) of $SrFe_{12-x-y}Co_xCr_yO_{19}$ ($0 \leq x, y \leq 1$) hexaferrites.	53
Table 3.3 Atomic weight %, average grain size (G_{avg}), bulk density (BD), and porosity (P) of $SrFe_{12-x-y}Co_xCr_yO_{19}$ ($0 \leq x, y \leq 1$) hexaferrites.	54
Table 3.4 Saturation magnetization (M_s), remanent magnetization (M_r), squareness ratio (M_r/M_s), coercivity (H_c), magnetocrystalline anisotropy field (H_a), and effective magnetic anisotropy (K_{eff}) of $SrFe_{12-x-y}Co_xCr_yO_{19}$ ($0 \leq x, y \leq 1$) hexaferrites at 300 K.	57
Table 3.5 Room-temperature value of dielectric constant (ϵ), tangent loss ($\tan \delta$), resistivity (ρ), and conductivity (σ) of $SrFe_{12-x-y}Co_xCr_yO_{19}$ ($0 \leq x, y \leq 1$) hexaferrites at 1MHz frequency.	60
Table 4.1 Structural parameters of $Sr_{1-x}Cr_xFe_{12-y}Zn_yO_{19}$ ($0 \leq x \leq 0.8$; $0 \leq y \leq 1$) hexaferrites.	66
Table 4.2 Characteristic absorption peaks [ν_1 , ν_2 (tetrahedral) & ν_3 (octahedral)] and bond length (r) of $Sr_{1-x}Cr_xFe_{12-y}Zn_yO_{19}$ ($0 \leq x \leq 0.8$; $0 \leq y \leq 1$) hexaferrites.	68
Table 4.3 Atomic weight %, average grain size (G_{avg}), bulk density (BD), and porosity (P) of $Sr_{1-x}Cr_xFe_{12-y}Zn_yO_{19}$ ($0 \leq x \leq 0.8$; $0 \leq y \leq 1$) hexaferrites.	69
Table 4.4 Saturation magnetization (M_s), remanent magnetization (M_r), squareness ratio (M_r/M_s), coercivity (H_c), magnetocrystalline anisotropy field (H_a), and effective magnetic anisotropy (K_{eff}) of $Sr_{1-x}Cr_xFe_{12-y}Zn_yO_{19}$ ($0 \leq x \leq 0.8$; $0 \leq y \leq 1$) hexaferrites at 300 K.	72
Table 4.5 Room-temperature value of dielectric constant (ϵ), tangent loss ($\tan \delta$), resistivity (ρ), and conductivity (σ) of $Sr_{1-x}Cr_xFe_{12-y}Zn_yO_{19}$ ($0 \leq x \leq 0.8$; $0 \leq y \leq 1$) hexaferrites at 1MHz frequency.	77
Table 5.1 Structural parameters of $SrFe_{12-x-y}Ni_xAl_yO_{19}$ ($0.005 \leq x \leq 0.02$; $1 \leq y \leq 4$) hexaferrites.	83
Table 5.2 Characteristic absorption peaks [ν_1 , ν_2 (tetrahedral) & ν_3 (octahedral)] and bond length (r) of $SrFe_{12-x-y}Ni_xAl_yO_{19}$ ($0.005 \leq x \leq 0.02$; $1 \leq y \leq 4$) hexaferrites.	85

Table 5.3 Atomic weight %, average grain size (G_{avg}), bulk density (BD), and porosity (P) of $SrFe_{12-x-y}Ni_xAl_yO_{19}$ ($0.005 \leq x \leq 0.02$; $1 \leq y \leq 4$) hexaferrites. 86

Table 5.4 Saturation magnetization (M_s), remanent magnetization (M_r), squareness ratio (M_r/M_s), coercivity (H_c), magnetocrystalline anisotropy field (H_a), and effective magnetic anisotropy (K_{eff}) of $SrFe_{12-x-y}Ni_xAl_yO_{19}$ ($0.005 \leq x \leq 0.02$; $1 \leq y \leq 4$) hexaferrites at 300 K. 88

Table 5.5 Room-temperature value of dielectric constant (ϵ), tangent loss ($\tan\delta$), resistivity (ρ), and conductivity (σ) of $SrFe_{12-x-y}Ni_xAl_yO_{19}$ ($0.005 \leq x \leq 0.02$; $1 \leq y \leq 4$) hexaferrites at 1MHz frequency. 92

Table 6.1 Structural parameters of $SrFe_8Al_4O_{19-x}Bi_2O_3$ ($0 \leq x \leq 5$ wt%) hexaferrites sintered at 1050°C temperature. 103

Table 6.2 Bulk density (BD), saturation magnetization (M_s), remanent magnetization (M_r), squareness ratio (M_r/M_s), and coercivity (H_c) of $SrFe_8Al_4O_{19-x}Bi_2O_3$ ($0 \leq x \leq 5$ wt%) with different sintering temperatures (850 to 1150°C) at 300K. 106

Table 6.3 Dielectric constant (ϵ), dielectric loss ($\tan\delta$), ac-resistivity (ρ), and ac-conductivity (σ) of $SrFe_8Al_4O_{19-x}Bi_2O_3$ ($0 \leq x \leq 5$ wt%) hexaferrites with different Bi_2O_3 content and at different sintering temperatures (850-1150°C) at 300K. 113

Table 7.1 Different phenomena and sources of magnetic anisotropy to tailor the coercive field of material. 117

Table 7.2 Structural parameters of $SrFe_{8-x}Al_4Zn_xO_{19}$ ($0 \leq x \leq 1$) hexaferrite. 119

Table 7.3 Characteristic absorption peaks [ν_1 , ν_2 (tetrahedral) & ν_3 (octahedral)] and bond length (r) of $SrFe_{8-x}Al_4Zn_xO_{19}$ ($0 \leq x \leq 1$) hexaferrites. 120

Table 7.4 Atomic weight %, average grain size (G_{avg}), bulk density (BD), and porosity (P) of $SrFe_{12-x-y}Ni_xAl_yO_{19}$ ($0.005 \leq x \leq 0.02$; $1 \leq y \leq 4$) hexaferrites. 122

Table 7.5 Saturation magnetization (M_s), remanent magnetization (M_r), squareness ratio (M_r/M_s), coercivity (H_c), magnetocrystalline anisotropy field (H_a), and effective magnetic anisotropy (K_{eff}) of $SrFe_{8-x}Al_4Zn_xO_{19}$ ($0 \leq x \leq 1$) hexaferrites at 300 K. 124

Table 7.6 Room-temperature value of dielectric constant (ϵ), tangent loss ($\tan\delta$), resistivity (ρ), and conductivity (σ) of $SrFe_{8-x}Al_4Zn_xO_{19}$ ($0 \leq x \leq 1$) hexaferrite at 1MHz frequency. 130

Table 8.1 A comparative evaluation of progress in energy density and other magnetic properties of modified SrM magnets (thesis work) with some commercially available strontium hexaferrite magnets. 140

List of Abbreviations and Symbols

BaM	Barium hexaferrite (BaFe ₁₂ O ₁₉)
<i>B</i>	Magnetic induction/ Magnetic flux density
<i>B_r</i>	Residual magnetic flux density/ Remanent flux density
(<i>BH</i>) _{max}	Energy product / Energy density
BD	Bulk density
<i>D</i>	Average crystallite size
Fe _A / Fe _B	Fe _(tetrahedral site) / Fe _(octahedral site)
<i>G_{avg}</i>	Average grain size
<i>H_a</i>	Intrinsic Coercivity
<i>H_c</i>	Magnetocrystalline anisotropy field
<i>K_{eff}</i>	Effective magnetocrystalline anisotropy
<i>M_r</i>	Remanent magnetization
<i>M_s</i>	Saturation magnetization
NdFeB	Neodymium-Iron-Boron magnet
PM	Permanent magnet
RE / REE	Rare earth / Rare earth elements
R _M	Fe ³⁺ /Sr ²⁺ molar ratio
SmCo	Samarium-Cobalt magnet
SrM	Strontium hexaferrite (SrFe ₁₂ O ₁₉)
<i>T_c</i>	Curie temperature
<i>T_f</i>	Functioning temperature
T _{ann}	Annealing temperature
T _{cal}	Calcination temperature
T _{sin}	Sintering temperature
<i>V</i>	Unit-cell volume
ε	Lattice strain
<i>χD</i>	X-ray density
ε	Dielectric constant
<i>tan δ</i>	Dielectric tangent loss
ρ	ac-resistivity
σ	ac-conductivity

PREFACE

Permanent magnets are a significant component in various applications like motor, wind turbine, generator, computer device, medical equipment, and many more. There is a huge demand for permanent magnets which was valued at \$17.85 Billion globally in 2018 and are expected to reach \$34.7 Billion by 2026. Among these magnets, NdFeB is the best performing magnet presently available in the market due to their high energy product. However, the market restriction and supply issues of rare-earth elements (REEs) due to the monopoly of China and the negative environmental effects of REEs extraction are demanding less dependency on REEs. It brings the challenge of developing a rare-earth free permanent magnet with high energy density.

Strontium hexaferrite (SrM) magnets represent the largest magnet group being used nowadays by volume. SrM is a ferrimagnetic material whose magnetic properties are inherently linked to the crystal structure and grain morphology. Though, it has a small energy density which is required to improve to reduce the dependency on NdFeB. Energy density is a key figure of merit, which is required to be high for better performance and is linked with the saturation magnetization (M_s) and coercivity (H_c) of the magnetic material. Due to high magnetocrystalline anisotropy, decent magnetism, chemical inertness, and high Curie temperature, these magnets are continuously drawing the attention of research communities to improve the low energy density of SrM with different means. It is found as the most faithful base magnet in terms of abundance and economic balance, which requires more or less reformation and advancement in the aspect of magnetic properties. Improvement in M_s and H_c of SrM magnet, even mildly, could open up the possibilities of large-scale immersion of strontium hexaferrite based magnets in numerous permanent

magnet applications. In the past several years, enormous improvement has been made toward enhancing the magnetic properties of SrM.

The thesis work is focused on the ‘development of rare-earth free permanent magnets with improved magnetic properties’, where the magnetic properties of strontium hexaferrites have been tried to improve toward the proposed objective. Detailed investigations on the structural, magnetic, and dielectric properties of five different SrM-based compositions (not reported earlier by other authors) have indicated a good improvement in SrM compositions. The results of different SrM-based series are briefly outlined here. It is arranged into nine chapters, and a brief description of each chapter is as follows:

Chapter 1 provides a brief introduction to permanent magnets and the different magnetic properties of a magnetic material. The featured characteristics of strontium hexaferrite magnets are discussed with the requirement of certain criteria that must be fulfilled for developing a permanent magnet. Concerning the significance of these criteria, literature surveys on the effect of synthesis techniques and current progress in magnetic properties of strontium hexaferrite magnets due to the substitution of various non-rare-earth elements are summarized in this chapter. Finally, it is concluded with the scope and objective of the present work.

Chapter 2 provides a detailed overview of the experimental techniques applied in the present thesis work. It includes sample preparation procedures and a detailed introduction to the working principles of different characterizing instruments that are used in the different studies of synthesized samples.

Chapter 3 presents the synthesis of a $\text{SrFe}_{12-x-y}\text{Co}_x\text{Cr}_y\text{O}_{19}$ ($0 \leq x, y \leq 1$) hexaferrite. The effect of Co-Cr substitution on the structural, magnetic, and dielectric properties of SrM is studied. XRD pattern confirms the formation of magnetoplumbite hexagonal

structure of SrM hexaferrite. Co ion substitution is found favorable to improve the M_s value with a drastic decrease in H_c , resulting in a soft magnetic behavior of samples. In contrast, Cr substitution is observed to significantly enhance the H_c value (almost double) without adversely affecting the M_s , resulting in a better hard magnetic behavior of strontium hexaferrite. Also, both these elements are found liable for improving the ac-resistivity of pristine strontium hexaferrite.

Chapter 4 presents the synthesis of a $\text{Sr}_{1-x}\text{Cr}_x\text{Fe}_{12-y}\text{Zn}_y\text{O}_{19}$ ($0 \leq x \leq 0.8$; $0 \leq y \leq 1$) hexaferrite. The effect of Cr-Zn substitution on the structural, magnetic, and dielectric properties of SrM is studied. XRD pattern confirms the formation of magnetoplumbite hexagonal structure of SrM hexaferrite. Cr substitution at Sr site is also found favorable to improve the H_c value but not as significant as observed at Fe site, with a slight decline in M_s value. Zn substitution at Fe site of SrM is observed to improve M_s value considerably with a drastic reduction in H_c value, resulting in a soft magnetic behavior of the sample. Despite the sharp H_c dilution due to Zn ion, Cr substitution retained the hard magnetic characteristic of samples by maintaining H_c value greater than at least 1 kOe. Also, both these elements are found liable for improving the ac-resistivity of pristine strontium hexaferrite.

Chapter 5 presents the synthesis of a $\text{SrFe}_{12-x-y}\text{Ni}_x\text{Al}_y\text{O}_{19}$ ($0.005 \leq x \leq 0.02$; $1 \leq y \leq 4$) hexaferrite. The effect of Ni-Al substitution on the structural, magnetic, and dielectric properties of SrM is studied. XRD pattern confirms the formation of magnetoplumbite hexagonal structure of SrM hexaferrite. Ni substitution is found favorable to improve the M_s value of samples without adversely affecting the H_c . Al substitution is observed to significantly increase the H_c value of SrM, even higher than NdFeB but at the cost of M_s value. Also, both these elements are found liable for improving the ac-resistivity of pristine strontium hexaferrite.

Chapter 6 presents the synthesis of a $\text{SrFe}_8\text{Al}_4\text{O}_{19-x}\text{Bi}_2\text{O}_3$ ($0 \leq x \leq 5$ wt%), where the doping effect of Bi_2O_3 sintering aid and the effect of different sintering temperature is studied on the structural, magnetic, and dielectric properties of Al-substituted SrM. XRD pattern confirms the formation of magnetoplumbite hexagonal structure of SrM hexaferrite. Mainly, the study of this chapter is motivated to compensate for the M_s loss in $\text{SrFe}_8\text{Al}_4\text{O}_{19}$ (a drawback of 4 Al substitution in SrM). The doping concentration of Bi_2O_3 and sintering temperature is optimized to realize better magnetic properties in $\text{SrFe}_8\text{Al}_4\text{O}_{19}$. Both Bi_2O_3 dopings and T_{sin} variation have reduced the ac-resistivity of samples compared to pristine strontium hexaferrite, but it is still higher than NdFeB.

Chapter 7 presents the synthesis of a $\text{SrFe}_{8-x}\text{Al}_4\text{Zn}_x\text{O}_{19}$ ($0 \leq x \leq 1$) hexaferrite. The effect of Al-Zn substitution on the structural, magnetic, and dielectric properties of SrM is studied. XRD pattern confirms the formation of magnetoplumbite hexagonal structure of SrM hexaferrite. Al substitution is observed to considerably increase the H_c value, even higher than NdFeB, but at the cost of M_s value. Zn substitution is found more prominent in improving the M_s of compositions but at little expense of H_c . An improvement in both M_s and H_c values is observed for small Zn substitution ($x = 0.2$). Zn substitution improves the ac-resistivity of Al-substituted SrM, but it is less than pristine strontium hexaferrite (still higher than NdFeB).

Chapter 8 presents the progress in energy density of the three best compositions of different series concerning the improvement in magnetic properties of strontium hexaferrite in comparison to the NdFeB. Three compositions from different series of the thesis work is selected here to demonstrate the enhancement in $(BH)_{\text{max}}$, due to their high H_c , either nearly approaching to the H_c of NdFeB (~ 15.07 kOe) or even higher than that. Also, Curie temperature analysis of these samples is given in this chapter to deliberate the operating temperature efficiency of synthesized permanent magnets.

Chapter 9 briefly summarizes the important findings of the thesis work. A decent improvement in magnetic properties of strontium hexaferrite magnets is deliberated here with the optimal amount of substituted element and optimization in synthesis factors. It also highlights the future scope of research on this material.

